Infrared signatures of hole and spin stripes in La$_{2-x}$Sr$_x$CuO$_4$

W. J. Padilla[*] and M. Dumm[†]

Department of Physics, University of California at San Diego, La Jolla, California 92093-0319, USA

Seiki Komiya and Yoichi Ando

Central Research Institute of Electric Power Industry, Komae, Tokyo 201-8511, Japan

D. N. Basov

Department of Physics, University of California at San Diego, La Jolla, California 92093-0319, USA

We investigate the hole and lattice dynamics in a prototypical high-temperature superconducting system La$_{2-x}$Sr$_x$CuO$_4$ using infrared spectroscopy. By exploring the anisotropy in the electronic response of CuO$_2$ planes we show that our results support the notion of stripes. Nevertheless, charge ordering effects are not apparent in the phonon spectra. All crystals show only the expected infrared active modes for orthorhombic phases without evidence for additional peaks that may be indicative of static charge ordering. Strong electron-phonon interaction manifests itself through the Fano line shape of several phonon modes. This analysis reveals anisotropic electron-phonon coupling across the phase diagram, including superconducting crystals. Due to the ubiquity of the CuO$_2$ plane, these results may have implications for other high temperature superconductors.

The nature of spin and/or charge stripes in the cuprates and their involvement to high-temperature (I) superconductivity are currently at the center of a debate in condensed matter physics.[1,2] The expression "stripes" is a general term indicating that spins and/or holes may arrange themselves in quasi-one-dimensional or more complicated self-organized patterns. The stripe-ordered state minimizes the energy of holes doped in an antiferromagnetic matrix, thus leading to an inhomogeneous state of matter.[3] Static one-dimensional (1D) charge stripes have been observed in the La$_{2-x-y}$Nd$_y$Sr$_x$CuO$_4$ (LNSCO) system[4] with complementary evidence from neutron and x-ray diffraction techniques. Although signatures of stripes by way of charge ordering have not been observed in La$_{2-x}$Sr$_x$CuO$_4$ (LSCO) and other high-temperature superconductors, there is evidence of the possible existence of dynamical stripes in these systems.[5] On the other hand, spin stripes have been discovered in LSCO[6] and many researchers agree upon their universality in high-T_c superconductors. However, a key issue regarding this new electronic state of matter concerns the role of stripes in relation to superconductivity, i.e., whether they are responsible for high-temperature superconductivity or a competing phase with it.

Signatures of quasi-one-dimensional behavior should be observable in optical spectroscopy. In particular, the lowering of symmetry due the formation of rigid charge density waves results is known to have dramatic implications for infrared (IR) active phonons.[7] Electronic 1D behavior can be directly probed by way of frequency dependent conductivity. An observation of the anisotropic conductivity in weakly doped LSCO is consistent with the notion of stripes.[8,9] Notably these observations imply deviations from a hypothetical model in which the stripes are rigid rivers of charge embedded within an antiferromagnetic background. Moreover, electronic and lattice fingerprints of 1D transport have not been systematically explored as a function of doping. The goal of this work is to apply infrared spectroscopy for the purpose of a detailed examination of spin and/or charge ordering effects in a series of well-characterized LSCO crystals.

Infrared spectroscopy is a mature and powerful technique[10] for the study of phonons[11,12] electron-lattice coupling,[13,14] anharmonicity,[15] and charge and spin ordered states[7] resulting from a lowering of electronic and magnetic symmetry. Since precise measurements can be carried out with miniature single crystals, IR spectroscopy further permits a survey of the electronic anisotropy, which is naturally expected due to the formation of stripes in cuprates. The inherent frequency dependent nature of IR spectroscopy coupled with temperature dependent measurements, allows one to determine characteristic energy scales associated with stripe formation as well as their T dependence.

Here we present a systematic in-plane spectroscopic investigation on a series of detwinned $(0 \leq x \leq 0.06)$ single crystals and twinned $(x=0.08)$ crystals of La$_{2-x}$Sr$_x$CuO$_4$, see Fig. 1. From the parent Mott insulator to the strontium doped superconducting samples $(x=0.06, 0.08)$ the in-plane electrodynamics are characterized by reflectance measurements using polarized light. Samples were coated *in situ* with gold or aluminum, and spectra measured from the coated surface were used as a reference. This method, discussed previously in detail,[16] allows one to reliably obtain the absolute value of the reflectance by minimizing the errors associated with nonspecular reflection and small sample size. The optical conductivity $\sigma_1(\omega)+i\sigma_2(\omega)$ and complex dielectric function $\varepsilon_1(\omega)+i\varepsilon_2(\omega)$ were determined from a Kramers-Kronig (KK) transformation of the reflectance data after extrapolation to low and high energies.[17] The samples are high quality single crystals grown by the traveling-solvent floating-zone technique,[18] and are cut into rectangular platelets with edges along the orthorhombic axes (typical size of 1.5×0.5
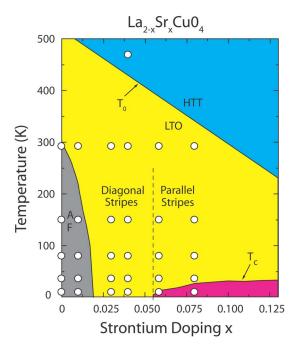
FIG. 1. (Color online). Phase diagram of LSCO. Circles indicate samples and temperatures characterized in this study. AF refers to the long range three-dimensional (3D) antiferromagnetic regime. The superconducting dome is indicated by the temperature T_c. The crystal structure HTT → LTO is also noted.

$\times 0.1 \text{ mm}^3$), where the c axis is perpendicular to the platelets within an accuracy of $1°$, as determined by x-ray Laue analysis.

One feature of this study compared to existing results is the utilization of detwinned single crystals. Previous studies of the phonon spectra used ceramic samples or twinned crystals, which makes the results inconclusive or hard to interpret. The possibility to produce detwinned single crystals of LSCO has been known for over a decade.[19] However, well-detwinned LSCO crystals have become available only after the recent finding that twin structures in these materials can be observed on a polished ac face under a microscope.[8,20] Hence there has yet to be a systematic investigation of the in-plane anisotropy as a function of temperature. A common shortcoming of existing studies is the lack of observation of all of the theoretically expected phonons in the LTO (low temperature orthorhombic) phase of LSCO. Some infrared studies of LSCO have supposed the reason for this was due to the fact that the transition to orthorhombicity was small[21] and had negligible effects on phonon/electronic structure, or that the presence of screening currents due to carriers obstructed their observation.[22] As will be shown, data for untwinned single crystals reported here allow us to remedy problems with earlier experiments.

It is instructive to discuss the phonon features of LSCO in the context of the evolution of the crystal structure as a function of temperature and doping. The phase diagram plotted in Fig. 1 is specific to LSCO, but many of the trends are generic for other cuprates. LSCO has two distinct crystallographic phases, a high-temperature tetragonal (HTT) phase, and a low-tmperature orthorhombic (LTO) phase. The separation between these two phases is denoted with the T_0 line in Fig.

TABLE I. Various notations used for labeling of the space groups and the subgroups of the K_2NiF_4 structure. The commonly used abbreviations are listed in the first column. The second column lists the Hermann-Mauguin notation, with the sequential numbers of space groups as given by the *International Tables for Crystallography* (Ref. 31), listed in parenthesis. The last column lists the Schoenflies equivalent notation.

Common Notation	Hermann-Mauguin	Schoenflies
high-T tetragonal (HTT)	$I4/mmm$ (139)	D_{4h}^{17}
low-T orthorhombic (LTO)	$Cmca$ (64)	D_{2h}^{18}
low-T tetragonal (LTT)	$P4_2/ncm$ (138)	D_{4h}^{16}
low-T orthorhombic 2 (LTO2)	$Pccn$ (56)	D_{2h}^{10}

1. The undoped crystal La_2CuO_4 (La214) is a Mott insulator and exhibits long range 3D antiferromagnetism (AF). As holes are added to the system by substitution of Sr^{2+} for La^{3+}, the AF quickly dies off and a superconducting phase is found for dopings $x \geq 0.055$. The dashed vertical line in Fig. 1 indicates the region where stripes are know to undergo a $45°$ rotation.[23] The open circles indicate each doping and temperature characterized in this study.

Insights into the expected number of IR active phonon modes in the LSCO system are provided by point group theory. LSCO belongs to a family of structures related to the K_2NiF_4 with space group D_{4h}^{17} (HTT) where the HTT phase can evolve into any of its Landau subgroups D_{2h}^{18} (LTO), D_{4h}^{16} (low-T tetragonal, LTT) and D_{2h}^{10} (low-T orthorhombic 2, LTO-2).[24–28] In Table I we summarize the various notations used for the different crystallographic phases of LSCO and related structures.

In LSCO the HTT→LTO transition is known to be of second order and occurs as a result of the bond length mismatch between the CuO_2 planes and the La_2O_2 bilayers. This mismatch is relieved by a buckling of the CuO_2 plane and a rotation of the CuO_6 octahedra (depicted in the lower panel Fig. 6) around the a_{ortho} axis, which is the reason for the structural change. Additionally, since the CuO_6 octahedra are tilted along the longer b_{ortho} axis, a reduction of symmetry compared to the HTT phase occurs and group theory predicts 17 infrared active phonons,[25,29,30] $\Gamma_{IR}=6B_{1u}+4B_{2u}+7B_{3u}$, i.e., seven modes along the b axis, four modes along the a axis, and six along the c axis. In contrast, the HTT phase has $\Gamma_{IR}=3A_{2u}+4E_u$, four modes parallel to the ab plane and three perpendicular to it. From this point on in the text we drop the "ortho" subscript notation as all axes referred to will be the LTO phase unless otherwise indicated.

Figure 2 displays the doping dependence of the reflectance $[R(\omega)]$ at $T=10$ K for both axes in the IR regime. In the undoped compound (red curves) relatively low values of $R(\omega)$ reveal its insulating nature and oscillations, due to IR active phonons, are observable in both axes and in all dopings studied. As holes are added to the Cu-O plane the overall reflectance increases smoothly and monotonically. At 6% doping (black curves), all phonon modes are still observable, and the high $R(\omega)$ values are indicative of metallic behavior.

In Fig. 3 we show the low-temperature infrared portion of the frequency dependent real conductivity, calculated from a
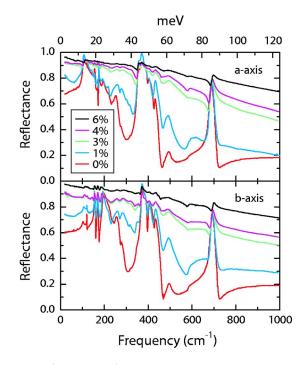
FIG. 2. (Color online). Infrared region of the low-temperature (10 K) reflectance for all detwinned crystals characterized. The a-axis spectra are displayed in the top panel and the b-axis results are shown in the bottom panel. The undoped parent compound (red curves) reveals its insulating character, and several IR active phonons can be observed in both axes. As carriers are added, the reflectance background increases monotonically to larger values.
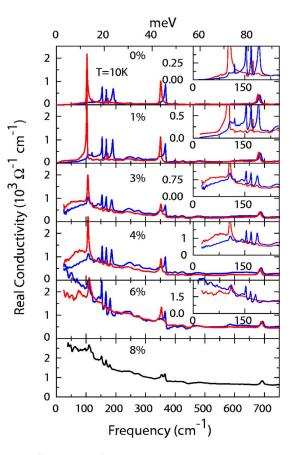

FIG. 3. (Color online). The infrared portion of the real conductivity for undoped $x=0$, top panel, and $x=0.01, 0.03, 0.04, 0.06,$ and 0.08 in the bottom panel. In the undoped compound (top) the a-axis data (red curves) display the expected four infrared active phonons and the b-axis spectra (blue curves) show the expected 7 IR active phonons. Insets detail the low frequency region and have the same horizontal and vertical units. All data are at $T=10$ K.

KK transformation of the data displayed in Fig. 2. In each panel the strontium doping is indicated, with the undoped parent compound La214 in the top panel and its superconducting counterparts $x=6\%,(T_c=8$ K$)$ and $x=8\%,(T_c=14$ K$)$ in the lower panels. The undoped parent compound exhibits low values of the conductivity consistent with its Mott insulating behavior. However the spectrum is punctuated by several strong phonons visible in both the a axis and b axis. As expected by point group analysis, we find four phonons in the a axis data at 103, 173, 351, and 679 cm^{-1} and seven phonons in the b-axis conductivity at 120, 155, 168, 191, 367, 399, and 684 cm^{-1}. A feature of this result is that *all* phonons expected from group theory analysis can be identified in the spectra for detwinned samples. Moreover, the complete set of phonon peaks is also found in the data for twinned superconducting crystals $x=0.08$ (bottom panel of Fig. 3).

We now turn to the analysis of the lineshape of phonon modes. Many resonances reveal an asymmetric line shape, (for an example, see Fig. 4). It is instructive to quantify the degree of asymmetry through the so-called Fano analysis. We model the asymmetric features of the real conductivity using the form given in Eq. (1),

$$\sigma_1 = \frac{S\omega}{4\pi}\left(\frac{(q\gamma+\omega-\omega_0)^2}{\gamma^2+(\omega-\omega_0)^2}-1\right),\qquad (1)$$

where S is the strength of the oscillator, γ is the damping, and ω_0 is the center frequency of the phonon. An asymmetric

phonon line shape is known to be related to electron-phonon coupling and is typically characterized through the Fano-Breit-Wigner (FBW) parameter q. The physical meaning of parameter q is that it is inversely related to the strength of the interaction.[33] The asymmetric line shape is general, and Fano derived a form for an oscillator coupled to an electronic continuum. These ideas were extended in Ref. 13 to include the interaction of a number of discrete states with that of a continua. The asymmetry in the line shape determines the energy range that the resonance is coupled. For example, a line shape that dips on the low-frequency (energy) side of the resonant frequency ω_0 indicates the phonon is interacting with a continuum at higher energies, where the sign of $1/q$ is positive in this case. For $1/q=0$ a phonon assumes a symmetric line shape and a Lorentz form is recovered.

In the left panels of Fig. 5 we quantify the degree of electron-phonon (el-ph) coupling, for both the a axis and b axis for all dopings characterized at $T=10$ K by plotting the doping dependence of $1/q$ parameter in Eq. (1). For the undoped parent compound, the $1/q$ parameter for the a-axis phonons is positive for all modes with the exception of the 685 cm^{-1} phonon. This result suggests that most of the a-axis modes interact with a continuum at higher energies
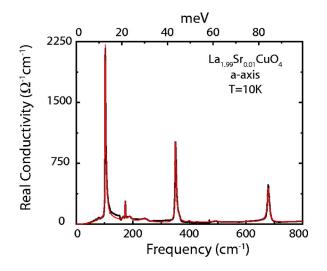
FIG. 4. (Color online). Frequency dependent real conductivity $\sigma_1(\omega)$ for 1% doped LSCO in the infrared regime (black curve). The coupling of the IR active phonons to an electronic continuum, evident here from their asymmetry, is visible for all four phonons. The red curve is a fit utilizing the Fano form for a resonance, listed in Eq. (1).

whereas the 685 cm^{-1} peak interacts with a continuum at lower energies. In contrast, all *b*-axis phonons in La214 interact with a continuum at lower energies.[34] As carriers are introduced, at 1% doping we find an abrupt switch to negative $1/q$ values for all *a* axis phonons. The *b*-axis phonons in the $x=0.01$ crystal do not show any anomalies. It should be noted that the 1% crystal is the only sample characterized in the AF regime in which the spin lies perpendicular to the *a* axis. The *el-ph* coupling relevant to the *a* axis spectra is essentially doping independent throughout the rest of the un-
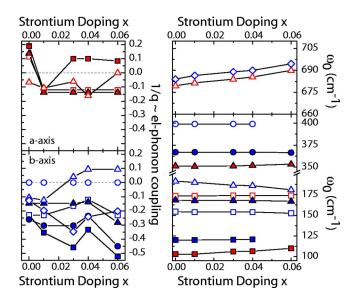

FIG. 5. (Color online). Left panels: the doping dependence of the Fano parameter ($1/q$), which is proportional to the electron phonon coupling; see text for a detailed description. Right panels: dependence of the center frequency of each IR active phonon vs doping. The symbols in the right panel denoting each phonon may be used as a key for the left panel. All data are at $T=10$ K.
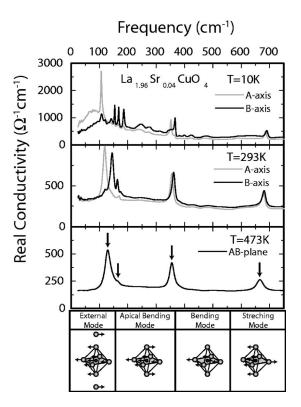

FIG. 6. Infrared region of $\sigma_1(\omega)$La$_{1.96}$Sr$_{0.04}$CuO$_4$ crystals at 10 K, room temperature, and in the HTT phase ($T=473$ K). The phonons for the HTT phase are indicated by arrows with the center frequencies given in the text. The bottom panel lists, in order from left to right, the assignment of each of these modes from low to high frequency as depicted by the CuO$_6$ octahedra. The temperature evolution of these modes can be tracked into the LTO phase displayed in the top two panels. Both the *a* axis (gray) and *b* axis (black) data in the LTO phase are plotted.

derdoped regime of the phase diagram, with the exception of the lowest energy phonon, which changes sign between 1% and 3%. The *b* axis phonons however, show significant signs of doping dependence and their $1/q$ values are roughly two to three times greater than those in the *a* axis. Lastly we notice that the values for $1/q$ in the 6% superconducting sample are similar to those crystals which do not exhibit superconductivity.

Let us examine directly the HTT to LTO transition through the spectra of the real conductivity. In Fig. 6 the infrared region of La$_{1.96}$Sr$_{0.04}$CuO$_4$ at 10 K, and 292 K along with the spectrum from the HTT phase ($T=473$ K) is shown. The HTT phase, as stated above, has four in-plane infrared active phonons and their normal modes are depicted in the lower portion of Fig. 6, while in the panel above, each mode is indicated by an arrow with their corresponding center frequencies at 129, 165, 355, and 666 cm^{-1}. It can be seen that some of these modes in the HTT phase split nearly symmetrically from their location into phonons in the *a* axis and *b* axis of the LTO phase. For example, the phonon at 355 cm^{-1} splits into the 352 cm^{-1} and 367 cm^{-1} phonons in the *a* axis and *b* axis respectively. The high-frequency phonon at 666 cm^{-1} hardens and splits into the phonons at 680 cm^{-1} (*a* axis) and 684 cm^{-1} (*b* axis). The splitting is such that the *a*-axis phonon always lies lower in frequency
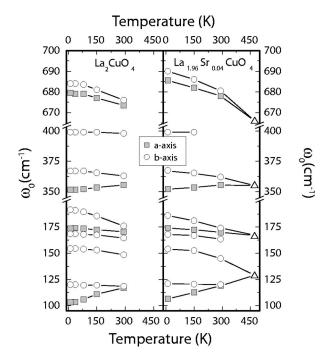
FIG. 7. Temperature dependence of the optically active phonons for undoped and 4% doped LSCO.
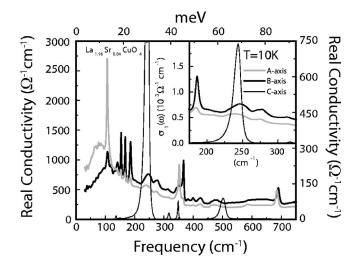

FIG. 8. Low-temperature infrared spectra measured for polarization of **E** vector along all three crystallographic axes for the LTO phase of $x=4\%$ Sr-doped LSCO. The a axis and b axis spectra (thick gray and thick black lines respectively) are shown in the main panel and their units correspond to the left coordinate. In order to display all phonons, the c-axis conductivity (thin black line) has been multiplied by a factor of 4 (right coordinate). The inset shows the c axis phonon at 244 cm^{-1} and the a axis and b axis all on the same vertical scale.

compared to the b-axis phonon in all dopings and temperature ranges characterized (also see the right panel of Fig. 7).

In Fig. 7 we show the temperature dependence of the center frequencies of all in-plane phonons for both the parent Mott-Hubbard insulator and for 4% LSCO. Many phonons are seen to be temperature independent with a few exceptions. The lowest frequency a-axis phonon at 120 cm^{-1} is seen to soften with decreasing temperature by nearly 15 cm^{-1}, while the b-axis phonon at 176 cm^{-1} hardens by the same amount. Phonons from the a axis and b-axis of the HTT bending mode at 355 cm^{-1} split symmetrically and soften and harden, respectively, by 4 cm^{-1} with the a-axis phonon lying lower in frequency. The high-frequency a-axis and b-axis phonons from the HTT stretch mode are seen to harden by about 7 cm^{-1}. Interestingly they also exhibit a significant doping dependence, as they both harden by 10 cm^{-1} from undoped compound to the superconducting 6% sample.

For completeness, we also show in Fig. 8 the c-axis data obtained for the $x=4\%$ LSCO crystal along with the a-axis and b-axis spectra, all at 10 K. As previously mentioned, one would expect six IR active modes in the c-axis in the LTO phase. In accord with this expectation we find phonons at 137, 151, 244, 317, 349, and 501 cm^{-1}. With this full characterization of lattice modes along all crystallographic orthorhombic axes, we can understand the origin of additional features seen for the in-plane measurements. For example, the structure near 250 cm^{-1} and 500 cm^{-1} in both the a axis and b axis spectra is likely to originate from the mixture of the c axis polarization. This unwanted effect is likely to be connected with roughness of the surface and/or minor miscut of the sample surface.[35] One can also observe unwanted leakage from the a axis to the b axis and vice versa, i.e., the triplet of phonons centered near 170 cm^{-1} in the b axis can be seen in the a axis data.

Let us now examine the anisotropy of the electronic background in the infrared conductivity data depicted in Fig. 3. As holes are added to the system by increasing the strontium doping, the conductivity increases and evolves smoothly and monotonically in both axes. We find that the electronic background shows substantial anisotropy in all untwinned samples with dopings $x \leq 6\%$.[36] This is in accord with transport measurements on detwinned single crystals of LSCO.[8] Enhancement of the conductivity occurs along the spin-stripe direction (a axis). This finding is therefore consistent with the notion of inherently conducting stripes. We also note that the anisotropy is greatest in the 1% crystal and is suppressed with the increasing doping. This result supports the relevance of spin stripes for the electronic transport in LSCO. Indeed, the separation between the stripes is enhanced at low dopings,[5] which inevitably should reduce the conductivity across the stripe direction.

We have shown a detailed temperature and doping dependent systematic investigation of the electromagnetic properties of the underdoped region of LSCO. The observation of all expected IR active modes as predicted by group theory indicates the quality of the samples studied here. It was found that all crystals exhibit line shapes suggestive of electron-phonon coupling. No anomalies in the electron-phonon coupling are found near 5% doping where the onset of superconductivity occurs in the phase diagram of LSCO. It is therefore safe to conclude that the superconducting phase boundary near $x=5\%$ is unrelated to modifications of the interaction between the doped holes and the lattice.

Electronic anisotropy evident in Fig. 3 supports the notion of stripes. For example, in all detwinned crystals, the low-temperature low-frequency limit of $\sigma_1(\omega)$ shows that the a axis has larger values, supporting the suggestion that stripes

are inherently conducting. The analysis of the phonon line shape calculated in the left panels of Fig. 5 shows stronger electron-phonon coupling along the *b* axis compared to the *a* axis. This in-plane *el-ph* anisotropy also supports the notion of stripes. The orthorhombicity in these systems was shown to be small and not sufficient to account for the values calculated here. Thus despite the two-dimensional nature of the layered CuO_2 planes, both the electronic conductivity and phonon line shape anisotropy are consistent with one-dimensional behavior and therefore support the notion of stripes.

The spectra of IR active phonons detailed in Fig. 3 show that all expected modes evolve smoothly and continuously as carriers are added to the system. This can be seen directly in the right panels of Fig. 5. Further the temperature dependence of the phonons vs temperature (Fig. 7) shows a continuous evolution. It must be noted that there are no indica-tions of new phonon modes anywhere in the underdoped region of the phase diagram. Also the temperature and dop-ing dependent evolution is linear with no signs of anhar-monic behavior. Since the lowering of crystal symmetry due to the formation of charge density waves results in a change in the number of IR modes and/or anharmonic behavior, the findings presented above rule this out. This result is incon-sistent with the notion of static charge ordering associated with spin stripes in LSCO. It is yet to be seen if the hypoth-esis of fluctuating stripes can account for our observations. As the CuO_2 plane is a common element to many high-T_c superconductors, these results may be important and more general than just limited to LSCO.

---

*Present address: Los Alamos National Laboratory, MS G756 MST-CINT, Los Alamos, NM 87545. Electronic address: willie@lanl.gov

†Present address: 1. Physikalisches Institut, Universität Stuttgart, 70550 Stuttgart, Germany.

[1] V. J. Emery, S. A. Kivelson, and J. M. Tranquada, Proc. Natl. Acad. Sci. U.S.A. **96**, 8814–8817 (1999).

[2] C. Castellani, C. Di Castro, and M. Grilli, Z. Phys. B: Condens. Matter **103**, 137 (1997).

[3] E. W. Carlson, V. J. Emery, S. A. Kivelson and D. Orgad, in *The Physics of Conventional and Unconventional Superconductors*, Vol. 2, edited by K. H. Bennemann and J. B. Ketterson (Springer-Verlag, NewYork, 2004).

[4] J. M. Tranquada, B. J. Sternlieb, J. D. Axe, Y. Nakamura, and S. Uchida, Nature **375**, 561 (1995).

[5] K. Yamada, C. H. Lee, K. Kurahashi, J. Wada, S. Wakimoto, S. Ueki, H. Kimura, Y. Endoh, S. Hosoya, G. Shirane, R. J. Birge-neau, M. Greven, M. A. Kastner, and Y. J. Kim, Phys. Rev. B **57**, 6165 (1998).

[6] S-W. Cheong, *et al.*, Phys. Rev. Lett. **67**, 1791 (1991); T. E. Mason *et al.*, *ibid.* **68**, 1414 (1992); T. R. Thurston, *et al.*, Phys. Rev. B **46**, 9128 (1992); K. Yamada, *et al.*, Phys. Rev. Lett. **75**, 1626 (1995).

[7] G. Grüner, *Density Waves in Solids* (Addison-Wesley, Reading, MA, 1994).

[8] Y. Ando, K. Segawa, S. Komiya, and A. N. Lavrov, Phys. Rev. Lett. **88**, 137005 (2002).

[9] M. Dumm, Seiki Komiya, Yoichi Ando, and D. N. Basov, Phys. Rev. Lett. **91**, 077004 (2003).

[10] D. N. Basov and T. Timusk, Rev. Mod. Phys. **77**, 721 (2005).

[11] A. Damascelli, K. Schulte, D. van der Marel, and A. A. Men-ovsky, Phys. Rev. B **55**, R4863 (1997).

[12] W. J. Padilla, D. Mandrus, and D. N. Basov, Phys. Rev. B **66**, 035120 (2002).

[13] L. C. Davis and L. A. Feldkamp, Phys. Rev. B **15**, 2961 (1977).

[14] S. Lupi, M. Capizzi, P. Calvani, B. Ruzicka, P. Maselli, P. Dore, and A. Paolone, Phys. Rev. B **57**, 1248 (1998).

[15] R. A. Cowley, Rep. Prog. Phys. **31**, 123 (1968).

[16] C. Homes, M. A. Reedyk, D. A. Crandels, and T. Timusk, Appl. Opt. **32**, 2976 (1993).

[17] F. Wooten, *Optical Properties of Solids* (Academic Press, New York, 1972).

[18] Y. Ando, A. N. Lavrov, S. Komiya, K. Segawa, and X. F. Sun, Phys. Rev. Lett. **87**, 017001 (2001).

[19] T. Thio, C. Y. Chen, B. S. Freer, D. R. Gabbe, H. P. Jenssen, M. A. Kastner, P. J. Picone, N. W. Preyer, and R. J. Birgeneau, Phys. Rev. B **41**, 231 (1990).

[20] A. N. Lavrov, S. Komiya, and Y. Ando, Nature **418**, 385 (2002).

[21] S. Tajima, T. Ido, S. Ishibashi, T. Itoh, H. Eisaki, Y. Mizuo, T. Arima, H. Takagi, and S. Uchida, Phys. Rev. B **43**, 10496 (1991).

[22] A. P. Litvinchuck, C. Thomson, and M. Cardona, in *Physical Properties of High-Temperature Superconductors IV*, edited by D. M. Ginsberg (World Scientific, Singapore, 1994).

[23] M. Matsuda, M. Fujita, K. Yamada, R. J. Birgeneau, M. A. Kast-ner, H. Hiraka, Y. Endoh, S. Wakimoto, and G. Shirane, Phys. Rev. B **62**, 9148 (2000).

[24] J. D. Axe, A. H. Moudden, D. Hohlwein, D. E. Cox, K. M. Mohanty, A. R. Moodenbaugh, and Youwen Xu, Phys. Rev. Lett. **62**, 2751 (1989).

[25] M. Napoletano, J. M. Gallardo Amores, E. Magnone, G. Busca, and M. Ferretti, Physica C **319**, 229 (1999).

[26] M. K. Crawford, R. L. Harlow, E. M. McCarron, W. E. Farneth, N. Herron, H. Chou, and D. E. Cox, Phys. Rev. B **47**, R11623 (1993).

[27] G. Burns, F. H. Dacol, D. E. Rice, D. J. Buttrey, and M. K. Crawford, Phys. Rev. B **42**, R10777 (1990).

[28] The Hermann-Maguin (H-M) space group notation used in the literature has been widely varying. For example the LTO phase has been represented by *Cmca* (Ref. 25), *Bmab* (Refs. 24 and 26), and *Abma* (Ref. 27). In space group notation for orthorhom-bic lattices, the *c* axis is taken to be the primary axis, and as such *Cmca* has been adopted as the standard H-M notation. However in this notation the *b* axis points perpendicular to the CuO_2 plane. Thus, much published work on high-T cuprates uses *Bmab* or *Abma* in an attempt to be consistent with the CuO_2

sheets lying in the *ab* plane. One may convert between these various notations [$Cmca \rightarrow Bmab \rightarrow Abma$] by changing the notation of the axes as [$abc \rightarrow a\bar{c}b \rightarrow cab$], respectively. In this work our assignment of the orthorhombic axes is consistent with the H-M notation *Bmab*. However, in order to avoid such complications, in this paper we use the crystallographic abbreviations, e.g., LTO, or the Shoenflies notation.

[29] R. Feile, Physica C **159**, 1 (1989).

[30] A. V. Bazhenov, C. B. Rezchikov, and I. S. Smirnova, Physica C **273**, 9 (1996).

[31] *International Tables for Crystallography, Vol. A: Space-Group Symmetry*, 4th edition, edited by Theo Hahn (Kluwer Academic Publishers, Boston, 1996).

[32] In addition to the asymmetric phonon fits, the electronic background as well as symmetric phonons, if any, are also fit in the real conductivity with Drude-Lorentz and Lorentz models respectively.

[33] U. Fano, Phys. Rev. **124**, 1866 (1961).

[34] The phonon in the *b* axis located near 400 cm^{-1} has a small oscillator strength, which makes the determination of the FBW constant arbitrary. Thus the asymmetric analysis has not been carried out for this phonon, as indicated by a $1/q=0$, i.e., a Lorentzian line shape.

[35] S. Tajima, S. Uchida, D. van der Marel, and D. N. Basov, Phys. Rev. Lett. **91**, 129701 (2003).

[36] This trend is reversed in the $x=6\%$ sample for which the *b*-axis conductivity is enhanced (bottom of Fig. 3). One caveat known from neutron measurements is that spin stripes undergo a 45 ° rotation at a strontium doping of $x=5.5\%$, above which the stripes lie parallel to the Cu-O bond direction; for example, see Ref. 23. Moreover, single crystals near $x=5.5$–6% doping commonly reveal the coexistence of diagonal and collinear stripes. It is likely that the anisotropic anomaly we find in the $x=6\%$ crystal may be related to complications resulting from the coexistence of the two forms of spin-stripe patterns.